Electronic Supplementary Material (ESI) for Journal of Materials Chemistry C.
This journal is © The Royal Society of Chemistry 2021

Supporting Information

Electron Spin as Fingerprint for Charge Generation and Transport in Organic Semiconductors

Alberto Privitera,[1]* Ross Warren,[1] Giacomo Londi,[2] Pascal Kaienburg,[1] Junjie Liu,[1] Andreas Sperlich,[3] Andreas E. Lauritzen,[1] Oliver Thimm,[4] Arzhang Ardavan,[1] David Beljonne,[2] Moritz Riede[1]*

[1] Clarendon Laboratory, Department of Physics, University of Oxford, Oxford OX1 3PU, England, UK
[2] Laboratory for Chemistry of Novel Materials, University of Mons, B-7000 Mons, Belgium
[3] University of Würzburg, 97074 Würzburg, Germany
[4] IEK5-Photovoltaics, Forschungszentrum Jülich, 52425 Jülich, Germany Experimental Physics VI, Julius Maximilian
E-mail: alberto.privitera@physics.ox.ac.uk, moritz.riede@physics.ox.ac.uk

Table of Contents:

SI-1 Neat ZnPc film

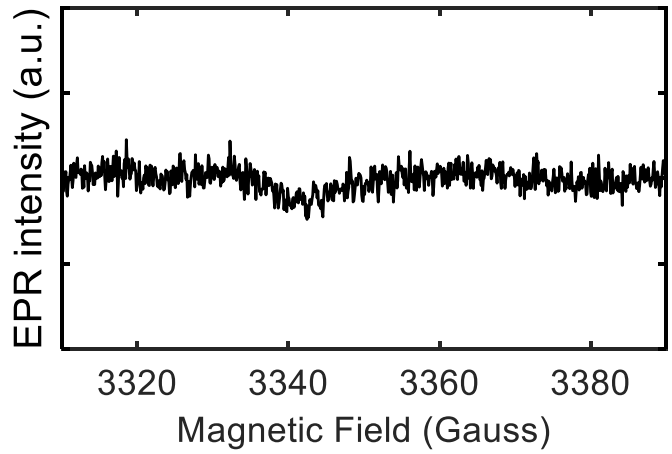

Figure SI1: cw EPR spectrum of neat ZnPc film recorded at 280K. The spectrum has been acquired with the following experimental parameters in accordance with all the EPR spectra reported in this manuscript: modulation amplitude = 1 G, microwave power = 0.2 mW (30 dB attenuation). The signal at 3330 Gauss has a very low EPR intensity and is attributable to the EPR cavity background.

SI-2 EPR Saturation Measurements

With the aim to understand whether the two peaks observed in Figure 2a are attributable to a single species with a pronounced g-tensor anisotropy or to two different species, we performed EPR power saturation measurements. In these measurements, the EPR spectrum is recorded at different MW powers such that different saturation behaviours of the detected species are probed. The EPR saturation spectra, recorded at 80K, are reported in Figure SI2. At low MW powers (MW attenuation: 45dB-25dB) no saturation of the EPR signal is observable and the intensity ratio of the two EPR lines remains constant. In contrast at higher MW powers (MW attenuation 20dB-5dB), a variation in the intensity ratio between the two peaks can be observed as well as a line broadening. The different saturation behaviour of the two peaks indicates the presence of at least two different species within the sample.

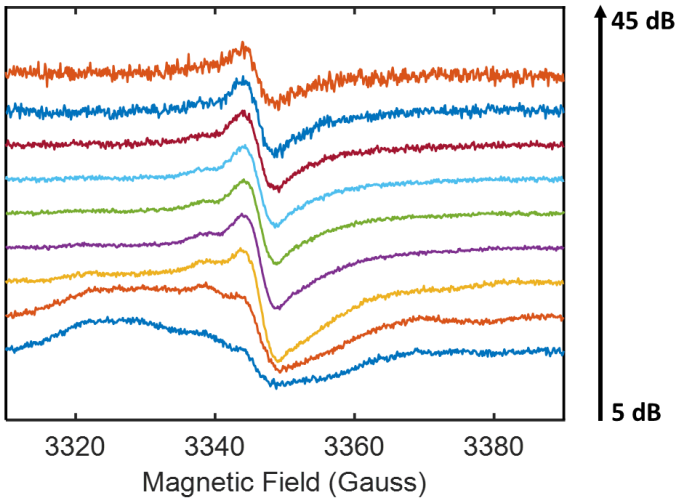

Figure SI2: Normalized cw EPR saturation measurements of ZnPc doped with 1 wt.% (MR=0.017) of F6-TCNNQ, recorded at 80K. The different spectra are recorded with microwave attenuation ranging from 5 dB (P_{MW}=63 mW) to 45 dB (P_{MW}=0.0063 mW) with steps of 5 dB. The shoulder at 3330 Gauss is due to the EPR signal of the cavity and is not further discussed below.

SI-3 DFT Analysis

The g-tensor values were calculated at the DFT PBE0/Def2-TZVP level of theory for a negative charged F6-TCNNQ molecule sandwiched between two neutral ZnPc molecules at a distance of 3.77Å from the anion. As a result, the excess charge and the spin density is localized on the F6-TCNNQ molecule.

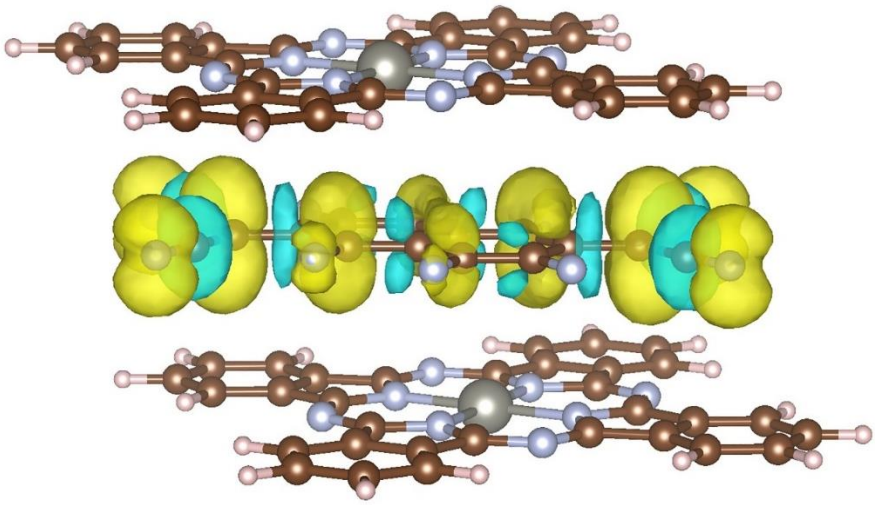

Figure SI3: Spin density distribution on a negatively charged F6-TCNNQ molecule between two neutral ZnPc ones. The yellow surface contour represents the spin α (positive) population, while the light-blue one the spin β (negative) population.

	g-values
$\mathbf{g_x}$	2.002632
$\mathbf{g_y}$	2.003463
$\mathbf{g_z}$	2.004160
$\mathbf{g_{iso}}$	2.003418

Table SI1: Computed g-values for the F6-TCNNQ radical anion (S=1/2).

SI-4 EPR Best-Fit Spectral Simulation

EPR best-fit spectral simulations allow determining important information regarding the g-tensor of the paramagnetic species, which in turn permits to unambiguously distinguish different species in the sample, and their line widths, which provide a wealth of information on transport dynamic at microscopic level. All the best-fit spectral simulations present in this manuscript were carried out using Easyspin (version 5.2.27), a Matlab™ toolbox for simulating and fitting EPR spectra.

Given the big number of parameters involved in the fitting of our samples, a few simplifications have been used to keep the number of fitted parameters as little as possible and thus obtain results which are more robust and reproducible. The details of the simulations are summarized in the following.

Firstly, since the g-value for the F6-TCNNQ anion is not present in literature, we used the values of the g-tensor obtained via DFT for all the simulations present in this manuscript (see SI-3). Conversely, the g-value of the ZnPc positive polaron was obtained from the spectral simulations taking into account the value reported in literature.[1]

Secondly, to simulate the peak-to-peak EPR line width of F6-TCNNQ anion a Voigtian broadening (Gaussian + Lorentzian) was used. The presence of Gaussian broadening is due to static effects such as orientational disorder and unresolved hyperfine splitting. The EPR line width was inferred from the EPR spectrum at 1 wt.% (MR=0.017) doping concentration acquired at 280K and kept constant for the EPR simulations at different temperatures and doping concentrations. This simplification allows to obtain a more robust and reliable fitting and is in line with the assumption of static F6-TCNNQ anions. Since we do not provide an exact value for the F6-TCNNQ anion line width though, we do not comment on its trend as a function of dopant concentration and temperature. Conversely, for the ZnPc positive polaron, just a Lorentzian broadening was considered, as an effect of the motional dynamics of ZnPc polarons which averages the inhomogeneous broadening contribution. It is worth underlining that no Dysonian contribution has been considered in our analysis since Dysonian lineshape arises only when the sample thickness is comparable or greater than the microwave skin depth, which is not the case for our samples. The EPR line width in this case was fitted using the EasySpin's function *esfit*.

Finally, also the weights of the two species were fitted using the EasySpin's function *esfit*. For the *esfit* fitting, the optimization algorithm we used is the Nelder/Mead downhill simplex method since it is more robust than Levenberg/Marquardt algorithm.

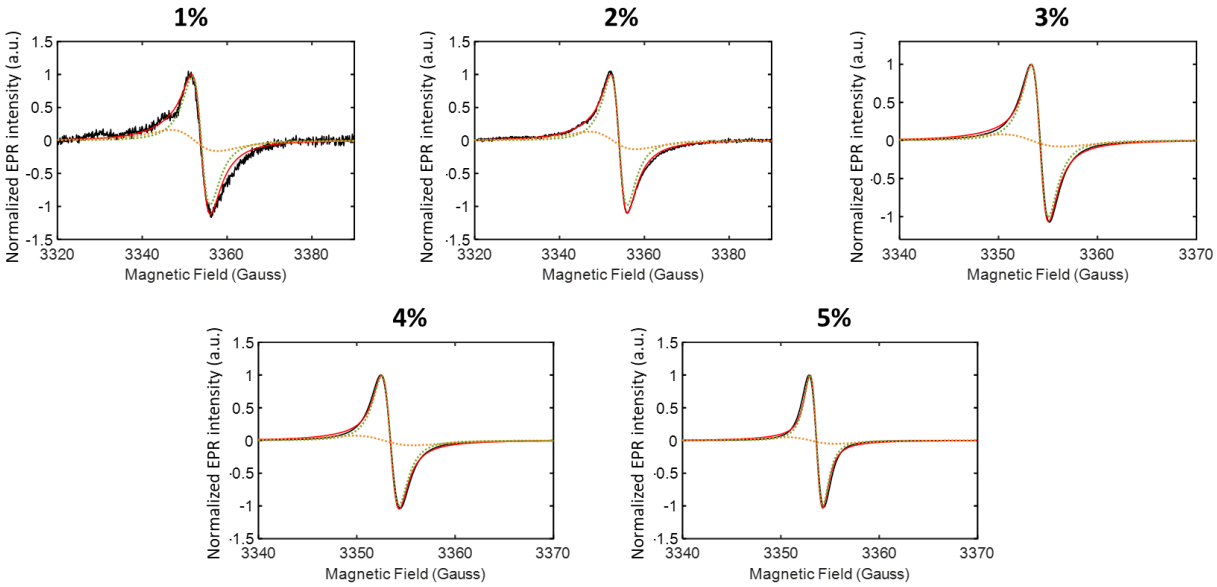

Figure SI4: Normalized experimental spectra at 280K (black lines) and spectral simulations (red lines) of ZnPc film doped with (a) 1, (b) 2, (c) 3, (d) 4, (e) 5 wt.% (MR=0.017-0.085) of F6-TCNNQ. The spectral simulation consists of the sum of two contributions: the F6-TCNNQ anion (orange line) and the ZnPc positive polaron (green line).

	F6-TCNNQ			**ZnPc**		
	g-tensor (DFT)	**[Gauss Loren] line width (mT) (EPR)**	**weight (fit)**	**g-value (EPR)**	**Lorentzian line width (mT) (fit)**	**weight (fit)**
1%	[2.0026 2.0034 2.0041]	[0.5 1] ± 0.2	0.45±0.05	2.0023 ±0.0005	0.45±0.02	0.55±0.05
2%			0.36±0.05		0.39±0.02	0.64±0.05
3%			0.18±0.05		0.18±0.02	0.82±0.05
4%			0.13±0.05		0.17±0.02	0.87±0.05
5%			0.07±0.05		0.12±0.02	0.93±0.05

Table SI2: g-values, EPR line widths in mT and relative weights obtained from the best-fit spectral simulations of the experimental spectra recorded at 280K reported in Figure SI4. The line widths are computed by convolving the final simulated field-swept stick spectrum with a Voigtian or Lorentzian line shape of a given width. For the F6-TCNNQ anion the simulation contains a Voigtian lineshape [Gaussian + Lorentzian], which was kept constant in all the simulations, while for the ZnPc positive polaron just a Lorentzian lineshape was considered, which was fitted. The weights of the EPR signals of both species were fitted using EasySpin's function *esfit*. Legend: DFT = value obtained from DFT calculations, EPR = value obtained from EPR simulation, fit = value obtained from *esfit* function. The errors have been estimated by running several fits with different initial conditions.

SI-5 Discussion on EPR Spectra at Different Doping Concentrations

In Figure 2b, the EPR spectra of ZnPc doped at different doping concentrations (1-5 wt.%, MR=0.017-0.085) recorded at 280K are shown. At low doping concentrations (1, 2 wt.%, MR=0.017, 0.034), the spectra clearly show the presence of two contributions which can be easily distinguished by "eye". At increasing doping concentrations though (3, 4, 5 wt.%, MR=0.052, 0.069, 0.085), the two species become difficult to distinguish. In particular, the EPR signal of the F6-TCNNQ anion seems to decrease in intensity. Different reasons can be figured out in order to rationalize this observation. In the following, we summarize and discuss the most significant hypothesis. Hypothesis 1, 2, 3 and 4 are ruled out after discussion and only hypothesis 5 is shown to be possible.

1) **The EPR signal of F6-TCNNQ anions shows MW power saturation at high doping concentrations:** To rule out this hypothesis, we carried out the EPR saturation measurements in the 3, 4 and 5 wt.% (MR=0.052, 0.069, 0.085) samples at two different temperatures (80K and 280K). The spectra show that no saturation occurs using a microwaves (MW) power of 0.2 mW (attenuation = 30 dB) neither at 80K nor at 280K. Since all the measurements presented in this manuscript were recorded with a MW power of 0.2 mW and therefore far from saturating conditions, the "disappearance" of the F6-TCNNQ anion signal cannot be ascribed to MW saturation.

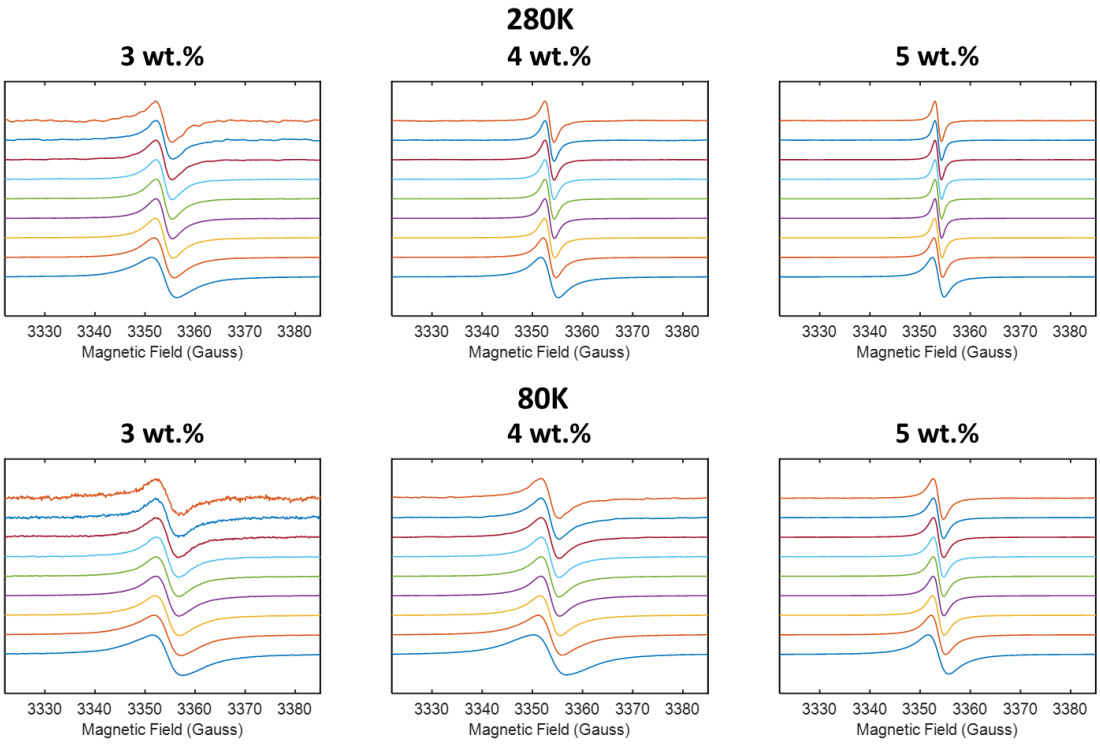

Figure SI5: Normalized cw EPR saturation measurements of ZnPc doped with 3, 4, 5 wt.% (MR=0.052, 0.069, 0.085) of F6-TCNNQ, acquired at 280K and 80K. The different spectra (from bottom to top) are recorded from 5 dB (P_{MW}=63 mW) to 45 dB (P_{MW}=0.0063 mW) with steps of 5 dB.

2) $F6TCNNQ^-/ZnPc^+$ CT state formation at high doping concentrations:

The formation of ion-pair complexes which have been previously observed in solution-processed doped organic semiconductors cannot rationalize the "disappearance" of the F6-TCNNQ anion line and therefore the ostensible presence of just one single EPR line in our EPR spectra at high doping concentrations.[2] On the one hand, ion-pair complexes are strongly exchange-coupled anion/cation pairs which appear as a single EPR line. This may be apparently in line with our observation of a single EPR line in the EPR spectrum. On the other hand, however, ion-pair complexes would possess a g-value which is centered at an average value between g=2.0023 (ZnPc positive polaron) and g=2.0034 (F6-TCNNQ anion), which is not in accordance with what we observe, since the position of our EPR line is the same as the ZnPc positive polaron without any shift of the g-value. For the g-value calculation we calibrated the magnetic field using the DPPH radical, whose g-value is known from literature (g=2.0036) and whose narrow EPR line width allows obtaining a more precise calibration. The signal of the ZnPc positive polaron in our samples remains always at the same position (g=2.0023) and there is no presence of new EPR lines in our spectra at high doping concentrations.

3) Delocalization of the anion's electron to form a $(F6TCNNQ\text{-}ZnPc)^-$ species

The delocalization of the unpaired electron present in the F6-TCNNQ anion to form a new $(F6TCNNQ\text{-}ZnPc)^-$ species would generate a new EPR signal with a g-value closer to the ZnPc one compared to the non-hybridized F6-TCNNQ anion. Nevertheless, this species is unlikely to generate given the huge difference in the LUMO orbitals of ZnPc and F6-TCNNQ which is one of the requirements for hybridization to occur. In addition, we do not observe any new species with a different g-value from ZnPc positive polaron in our spectra at high doping concentrations.

4) $F6TCNNQ^{2-}$ di-anion formation

The generation of a di-anion localized on the F6-TCNNQ molecule might rationalize the disappearance of the anion EPR signal at high doping concentrations. The di-anion of F6-TCNNQ, indeed, is diamagnetic (S=0) which means that it doesn't show any EPR signal.[3] However, the generation of di-anions at high doping concentrations is quite unlikely for two main reasons. Firstly, the presence of a di-anion would suggest a doping efficiency higher than 100% for ZnPc doped with F6-TCNNQ which to our knowledge has never been observed in literature for ZnPc doped with F6-TCNNQ. This point is further corroborated by our quantitative analysis which show a doping efficiency lower than 100%. (see section SI-6). Secondly, the second electron affinity of F6-TCNNQ is much higher in energy than the ZnPc ionization potential and the F6-TCNNQ di-anion is reported to act as a strong donor.[3] This result definitely rules out the formation of F6-TCNNQ di-anions.

5) Antiferromagnetic coupling of F6-TCNNQ di-anion dimers

At high doping concentrations, the probability of dopant molecules clustering becomes higher. If two F6-TCNNQ molecules are sufficiently close to each other, the two unpaired electrons localized on the respective F6-TCNNQ anions can magnetically interact between each other. This results either in an antiferromagnetic ($J<0$) or ferromagnetic ($J>0$) coupling. In the case of antiferromagnetic coupling, the low energy state is a singlet ($S=0$) which does not show any EPR line. The antiferromagnetic coupling scenario has been confirmed by our theoretical DFT calculations.

To summarize, after having ruled out the most likely mechanisms, we tentatively conclude that at higher doping concentrations, the EPR signal of the F6-TCNNQ anion decreases in intensity because of an antiferromagnetic coupling mechanism which pair most of the unpaired anions in a singlet state that is EPR silent. Further details can be found in the main text.

SI-6 EPR Quantitative Analysis

EPR intensity (double integral of the EPR line) is proportional to the number of spins in the sample:[4]

$$Double\ Integral = c \cdot [G_R \cdot C_t \cdot n] \cdot \left[\frac{\sqrt{P} \cdot B_m \cdot Q \cdot n_B \cdot S \cdot (S+1)}{f(B_1, B_m)}\right] \cdot n_S$$

where c is a constant, G_R is the receiver gain, C_t is the conversion time, n the number of scans, P the microwave power, B_m the modulation amplitude, Q the quality factor of the cavity, n_B the Boltzmann factor for the temperature dependence, S the total electron spin, $f(B_1,B_m)$ a spatial distribution of the MW field and modulation field experienced by the sample and n_S the number of unpaired electron spins. By using a TEMPO-reference sample with a known number of spins, it is possible to calibrate the EPR spectrometer intensity and consequently calculate the absolute number of unpaired spins in our samples.

To do so, the following precautions have been considered.

1) We carried out all the EPR measurements keeping G_R, C_t, P (non-saturating conditions) and B_m (1 Gauss) constant. The total electron spin S is the same (S=1/2) for all the studied samples.
2) For each sample, we normalized the spectra over the number of scans.
3) The quality factor Q does not change significantly in our samples (standard deviation around 10% without any trend as a function of doping concentration). We took into account the standard deviation when estimating the error bars of the EPR intensity.
4) We assumed $f(B_1,B_m)$ constant for all our samples despite small changes due to the different conductivities of the samples which we took into account when we estimated the error bars.
5) We calibrated the spectrometer for each temperature we used so that we took into account the n_B parameter in our quantitative analysis.

From the calibration, we therefore obtained:

$$Double\ integral = const(T) \cdot n_S$$

which allowed us to obtain the absolute number of spins in our samples. The total spin concentration was then calculated by dividing the total number of measured spins by the sample volume. Finally, taking into account the weights of the EPR intensities of both the ZnPc positive polarons and the F6-TCNNQ anions, which were obtained by the best-fit spectral simulation, we calculated the concentration for each paramagnetic species (Figure 2c) and, as a result, the charge transfer efficiency (Figure SI6). The uncertainty with respect to the doping concentration was estimated based on the uncertainty of the QCM during the evaporation process. The uncertainty with respect to the absolute number of unpaired spins is less than 20% and was estimated based on the uncertainty of the volume and the concentration of the TEMPO-reference sample, the standard deviation of the quality factor Q and the uncertainty in $f(B_1,B_m)$.

SI-7 Photothermal Deflection Spectroscopy

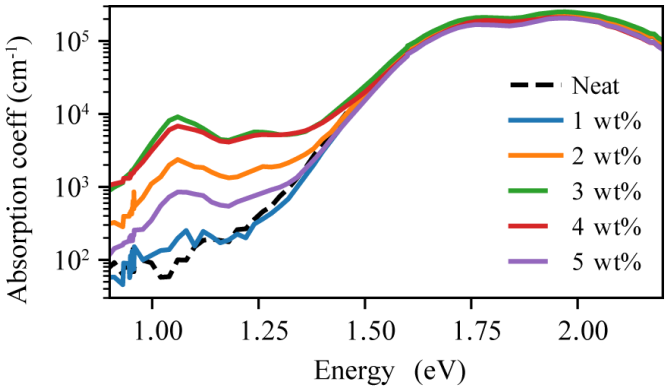

Figure SI6: PDS spectra of ZnPc films doped with F6-TCNNQ at different doping concentrations (0-5 wt.%, MR=0-0.085) acquired at room temperature. PDS technique is much more sensitive than UV-vis measurements in the low-absorption regime which is the spectral region of interest for our analysis. We therefore adopted this technique instead of standard UV-vis measurements which are more reliable in the high absorption region.[5]

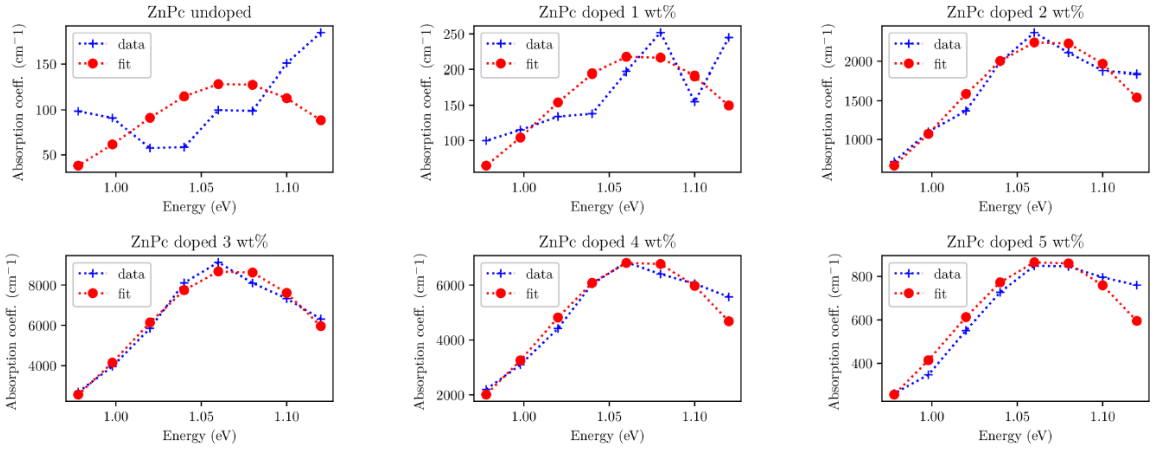

Figure SI7: Least squares fits of the F6-TCNNQ anion peak of the PDS spectra reported in Figure SI6. A Gaussian function has been used to fit the peaks, $g = ae^{-\frac{(x-x_0)^2}{2\sigma^2}}$, where a is the Gaussian height, x_0 is the position and σ is the width. The position and the width have been obtained by the 3 wt% fit and fixed for all the other concentrations: $x_0 = 1.069 \pm 0.002\ eV$, $\sigma = 0.058 \pm 0.003\ eV$.

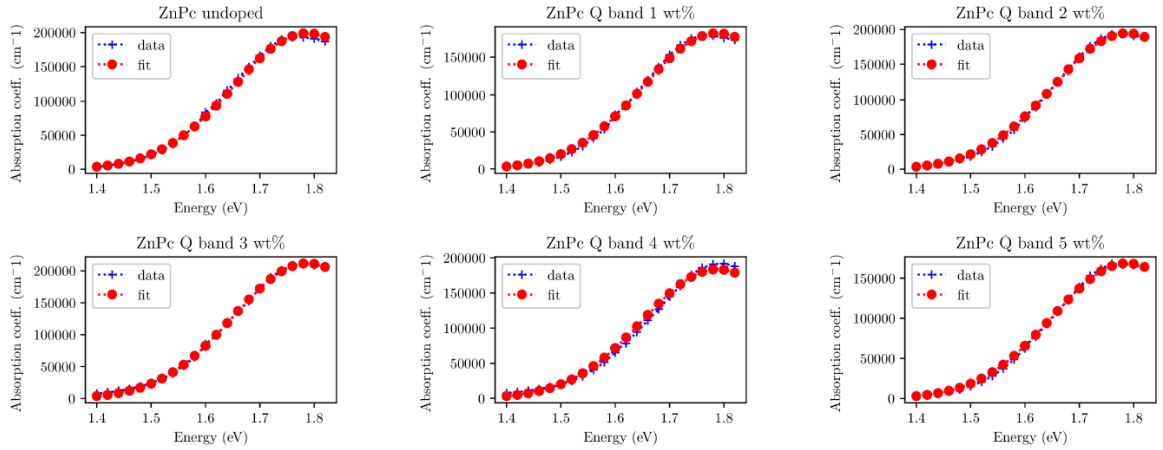

Figure SI8: Fitting of the Q-band peak of the PDS spectra reported in Figure SI6. Similarly to Figure SI7, a Gaussian model has been used to fit the Q-band peak at 1.78 eV (696 nm), $g = ae^{-\frac{(x-x_0)^2}{2\sigma^2}}$, where a is the Gaussian height, x_0 is the position and σ is the width. The position and the width have been obtained from the 3 wt% fitting and fixed for all the other concentrations: $x_0 = 1.788 \pm 0.002\ eV$, $\sigma = 0.137 \pm 0.002\ eV$.

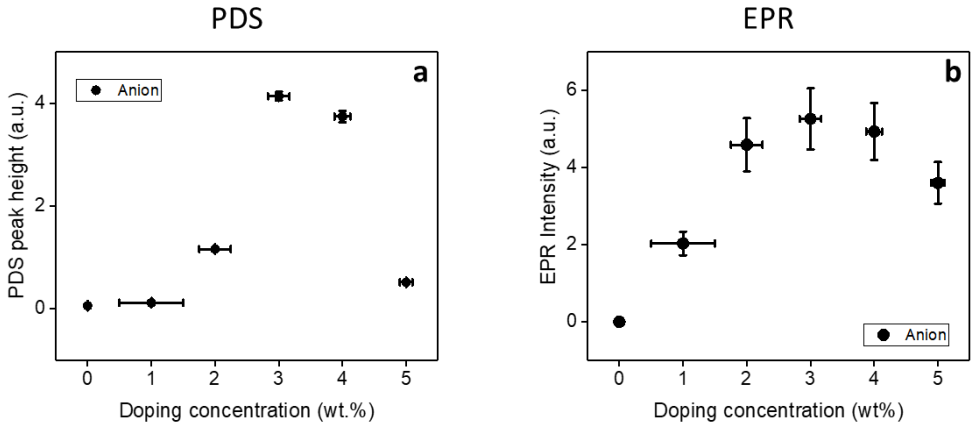

Figure SI9: (a) Relative peak height of the feature at 1.06 eV (1170 nm) of the PDS spectra reported in Figure SI7 as a function of doping concentration (0-5 wt.%, MR=0-0.085). This feature is attributed to the F6-TCNNQ anion in accordance to what was reported previously.[5] The peak height is calculated by fitting the peak at 1.06 eV with a Gaussian function. The peak height of the fit is scaled relatively to the intensity of the Q-band absorption peak at 1.78 eV (696 nm) and multiplied by 100. (b) EPR intensities of the EPR signals of the F6-TCNNQ anion as a function of doping concentration. The EPR intensities are calculated via EPR quantitative analysis of the spectra in Figure 2b (further information in section SI-6). Notably, PDS and EPR analyses show similar trends for the F6-TCNNQ anions. While as discussed in SI5, EPR trend can be explained by the presence of antiferromagnetic coupling mechanism at higher doping concentrations, the PDS trend can be rationalised considering that the new di-anion dimers possess a different absorption compared to the isolated anion.

SI-8 Statistical simulations

The antiferromagnetic model proposed in this manuscript occurs only if dopant molecules are close enough to each other. Over the concentration range considered (MR=0-0.85), a random distribution of dopants in the lattice would lead to a steady increase of the EPR signal of the anion, which would be at odds with our experimental data. To investigate this further, we built a simple 1D model to calculate the number of isolated dopants (those without another dopant molecule as a nearest neighbour) vs molar ratio. A simple 1D model has been adopted, since in the first instance we are interested in the z-direction (pi-pi stacking), which is the one along which the proposed antiferromagnetic coupling mechanism occurs. We compare the randomly distributed case, where all sites in the 1D lattice have an equal probability of being a dopant site, to a model where we capture a tendency for dopant clustering by generating a random dopant site from a Gaussian distribution with varying sigma (σ). In this case, we observe the number of isolated dopants increasing at low doping concentrations but decreasing towards higher concentrations. This behaviour results in the distinct maximum that is in agreement with our EPR results, as reported in Figure SI8. Therefore, our results suggest that the dopant is not homogeneously distributed, but rather it prefers to cluster.

Although the study of the dopant distribution within the host material is a difficult task since morphological techniques can hardly draw straightforward conclusions regarding this point, many studies provide a physical origin for dopant clustering. A few works are present in literature where e.g. via combined photoemission, high resolution TEM and electrical analysis they could indirectly infer interesting information about the dopant aggregation in systems which are similar to the one studied in our manuscript, namely CuPc p-doped with either TCNQ or WO_3.[6] In their study, they show that models developed for singly dispersed dopant molecules cannot be applied in order to describe the doping induced variations of the host matrix Fermi level. This has led them to take into account phase segregation to rationalise their data. Phase segregation is indeed well-known and commonly accepted by the scientific community in the case of p-type dopants based on metal oxides (e.g. MoO3),[7] however a similar analysis has not been discussed in detail yet in the case of organic dopants. Nevertheless, in several cases low doping efficiencies are attributed to the formation of clusters of dopant molecules.[8, 9]

In addition, further literature disclose that for effectively doped polycrystalline films dopant concentration is not supposed to be homogeneous.[10] For example, in PBTTT doped with F4TCNQ it has been observed that dopant molecules are incorporated into the side chain regions without disturbing the semicristalline lamellar chain pi-stacking of the polymer backbones. A similar result is also quite likely in evaporated systems where pure crystalline grains are thermodynamically stable and a preferable dopant distribution can be found in the grain boundaries.

Finally, further studies carried out on TCNNQ derivatives disclose that TCNNQ anions can arrange following different patterns depending on the intermolecular pi-pi interactions within the film, and most of the patterns include the presence of TCNNQ dimers with a molecular separation as close as 3.1 A between opposing monoanions.[3]

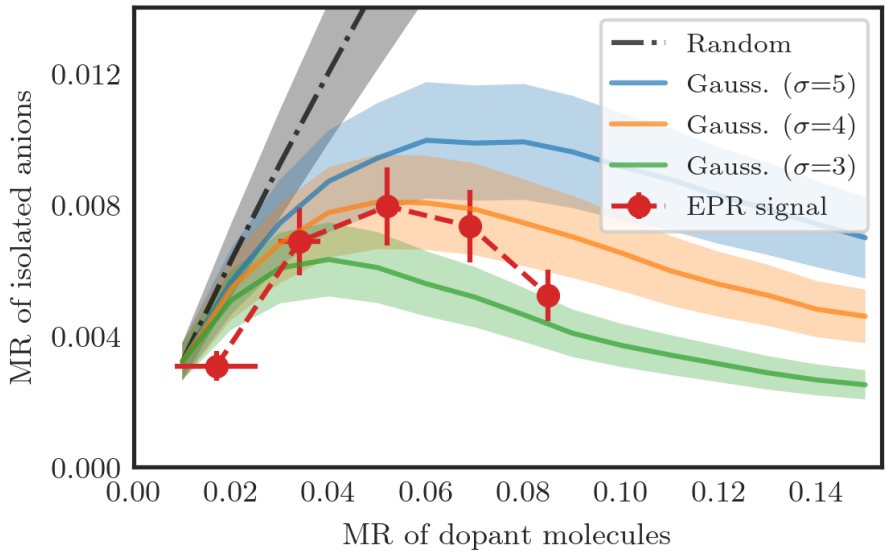

Figure SI10: Comparison of the MR of isolated anions as obtained by statistical simulations (coloured lines) and EPR analysis (red dots) as a function of MR of dopant molecules. The statistical simulations have been performed taking 100 "host sites" disposed in one dimension (pi-pi stacking) and using a random or gaussian distribution to assign the different sites (host or dopant) in line with the chosen MR. The process has been repeated 5000 times and the average has been taken. The error bars to the model represent the error on the doping efficiency measurements taken from our previous work and assuming it constant across all the studied concentrations.[11]

SI-9 DFT calculations on antiferromagnetic coupling

As discussed in the main text, DFT calculations were performed on two negatively charged F6-TCNNQ molecules in the Broken Symmetry (BS) formalism at the DFT PBE0/Def2-TZVP level of theory. As a first step, we placed one F6-TCNNQ molecule on top of the other at a distance of 3.77 Å along the z axis and we progressively increased up to ~5 Å and decreased down to ~2.5 Å this distance, in order to evaluate the variation of the $\Delta E_{T\text{-}S}$ as a function of the distance. According to the obtained values and trend (Figure SI9), we chose to further investigate the scenarios at three different distances, 3.00 Å ($\Delta E_{T\text{-}S}$ = 0.823eV, main text), 3.57 Å ($\Delta E_{T\text{-}S}$ = 0.113eV) and 3.77 Å ($\Delta E_{T\text{-}S}$ = 0.055eV). By keeping fixed the cartesian coordinates of one F6-TCNNQ molecule, we shifted the other along x with respect to its original position, from 0 to 6 Å with a pace of 1 Å. For each step along x, we displaced the same molecule also along y with respect to its original position, from 0 to 3 Å with a pace of 0.5 Å. For all the probed 7x7 configurations we assessed the energy difference between the triplet state and the singlet one, producing two different 2D contour plots (one is reported in the main text, the other below in Figure SI10). The results in both cases show that when two F6-TCNNQ molecules are close to each other, the probability for the triplet state to be higher in energy with respect to the singlet state is high when the relative displacement of the second molecule is less than 3.5 Å along the x axis and less than 3 Å along the y axis. In such cases, yet with some exceptions, the two magnetic centres are antiferromagnetically coupled. As regards the F6-TCNNQ molecule, we resorted to its crystallographic structure in Ref.[12]

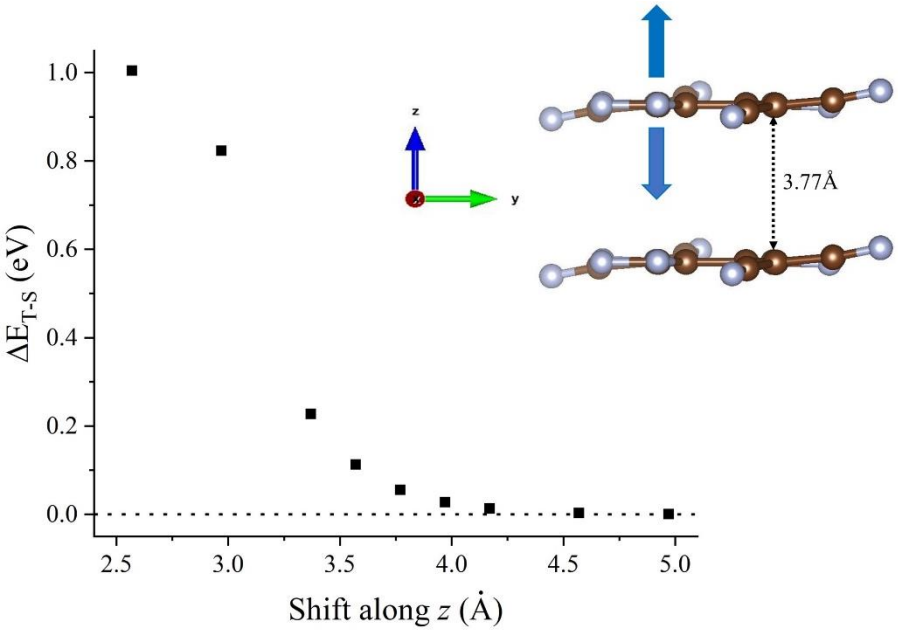

Figure SI11: Energy difference between the triplet and the singlet state ($\Delta E_{T\text{-}S}$) of two negatively charged F6-TCNNQ molecules as a function of their distance along the z axis.

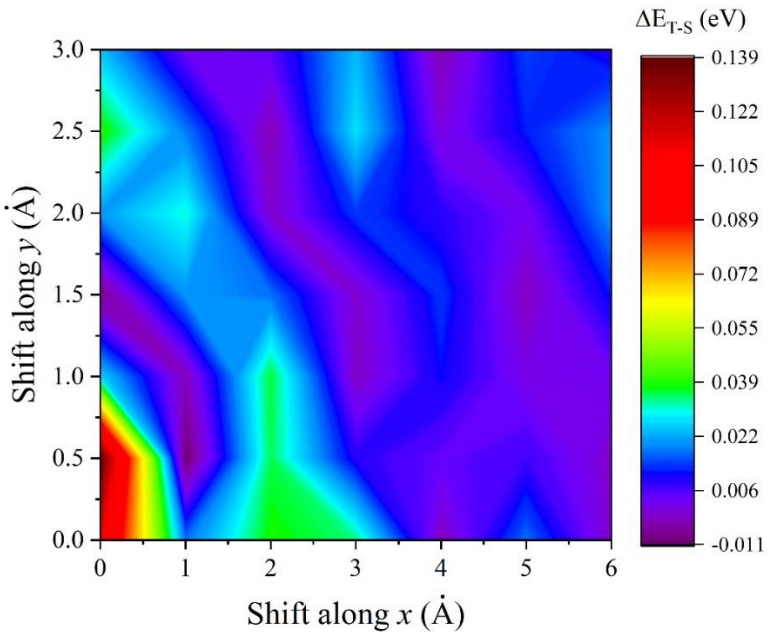

Figure SI12: 2D contour plot of ΔE_{T-S} of two coupled electrons localized on nearby F6-TCNNQ molecules, as a function of the x and y relative displacement of one molecule with respect to the other. The two molecules are distant by 3.57Å along the z axis for this simulation.

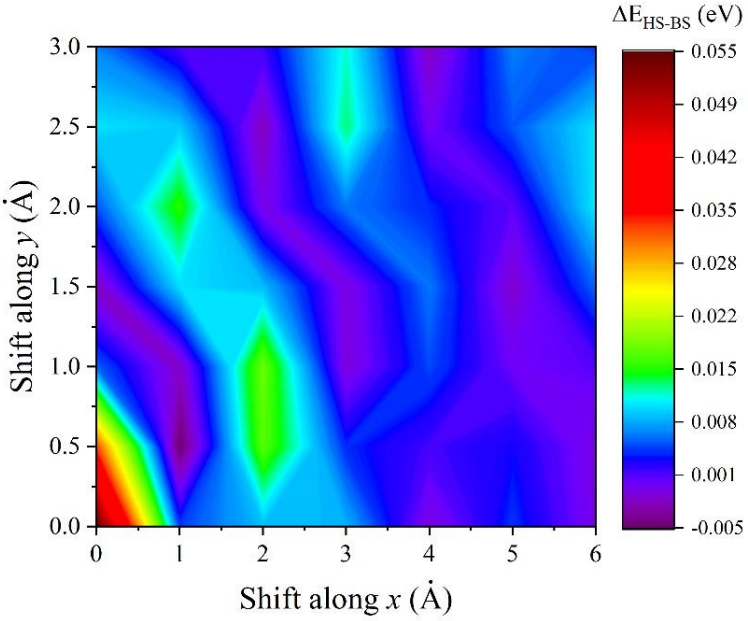

Figure SI13: 2D contour plot of ΔE_{T-S} of two coupled electrons localized on nearby F6-TCNNQ molecules, as a function of the x and y relative displacement of one molecule with respect to the other. The two molecules are distant by 3.77Å along the z axis for this simulation.

SI-10 Conductivity Discussion

Conductivity in p-doped semiconductors is defined as $\sigma = pe\mu$ where p is the density of free positive polarons, e is the electron elementary charge (e = $1.602 \cdot 10^{-19}$ C) and μ is the macroscopic mobility of the polarons.

Multiplying the conductivity by $\frac{N_{CT}^{+}+p}{N_{CT}^{+}+p}$, where N_{CT}^{+} is the density of positive polarons bound in the charge transfer state, the following equation is obtained:

$$\sigma = \frac{e\mu}{1 + \frac{N_{CT}^{+}}{p}} \left(N_{CT}^{+} + p\right)$$

In Figure 3c, we report the conductivity as a function of $(N_{CT}^{+} + p)$ calculated using EPR spectroscopy. From the best linear fit, carried out using $A = e\mu / \left(1 + \frac{N_{CT}^{+}}{p}\right)$, we obtain the following values:

A = $(4.5 \pm 0.2) \cdot 10^{-27}$ Sm^2

Adj. R-Square = 0.984

The strong linear correlation (highlighted by an adj. R-Square value very close to 1) underlines that neither the $\frac{N_{CT}^{+}}{p}$ ratio nor the macroscopic polaron mobility μ significantly change in the studied layers, since it is unlikely that the two effects cancel out. This result is in line with Tietze model which shows that $\frac{N_{CT}^{+}}{p}$ ratio is constant in the studied doping range.[7] In addition, since the macroscopic mobility does not significantly change in the studied doping range, the increase of the conductivity as a function of doping concentration can be attributed completely to the change in the density of free polarons.

From the A value it is possible to obtain a rough estimate of the macroscopic mobility in our films. Considering the ratio $\frac{N_{CT}^{+}}{p} \cong 20$, which is a good approximation in accordance with Tietze model,[13] we obtain $\mu \cong 6 \cdot 10^{-3}\ cm^2/Vs$ which is comparable with FET mobility values measured in literature for similar systems.[14]

SI-11 EPR Analysis at Different Temperatures

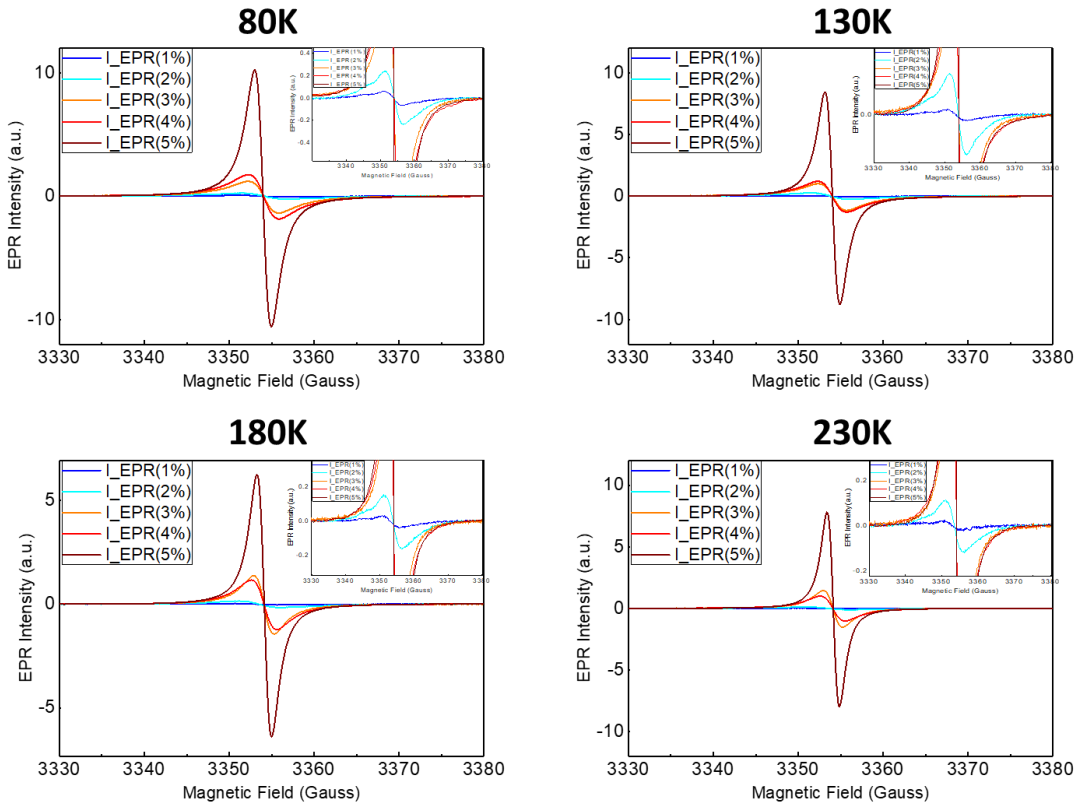

Figure SI14: cw EPR spectra of ZnPc doped with F6-TCNNQ at different concentrations (1-5 wt.%, MR=0.017-0.085) recorded at different temperatures (80K, 130K, 180K, 230K).

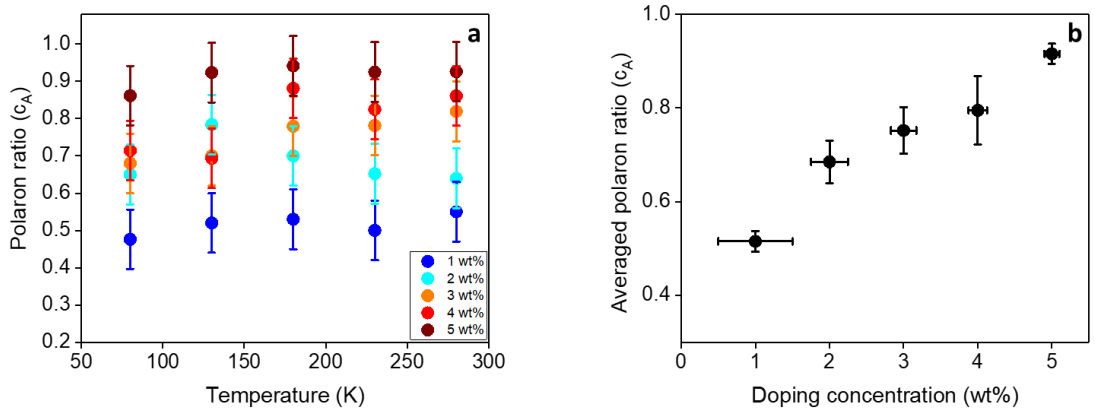

Figure SI15: (a) Relative weight of the EPR intensity of ZnPc positive polarons obtained from the best-fit spectral simulations of EPR spectra in Figure SI11. The value c_A $\left(c_A = \frac{p+N_{CT}^{+}}{p+N_{CT}^{+}+N_A^{-}}\right)$ does not significantly depend on the temperature but only on the doping concentration. From c_A, c_B can be easily obtain by 1-c_A. (b) Averaged values of c_A as a function of doping concentration. The average is carried out for the values of c_A at different temperatures.

	A (Curie term)	*B (Pauli term)*
1%	180 ± 100	0.7 ± 1.0
2%	850 ± 400	4 ± 3
3%	2400 ± 400	13 ± 3
4%	4400 ± 600	10 ± 4
5%	9800 ± 500	10 ± 3

Table SI3: Best-fit values obtained from the linear fit of the EPR intensities in Figure 3a as a function of the inverse of the temperature (I_{EPR}=A/T+B).

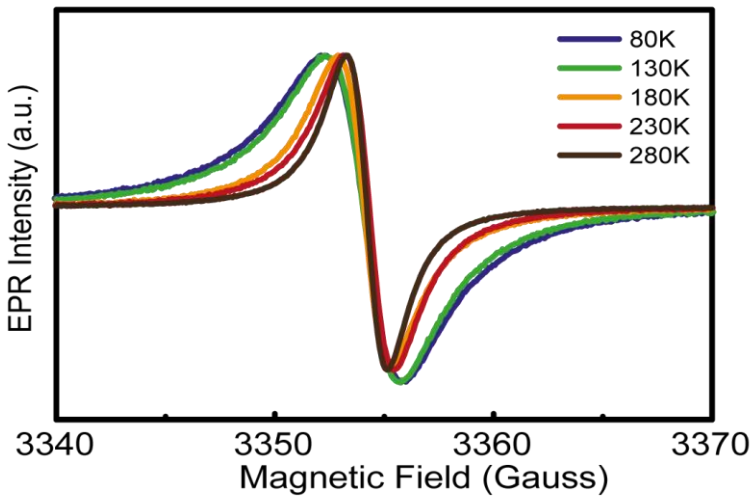

Figure SI16: cw EPR spectra of ZnPc doped with 3 wt.% (MR=0.052) of F6-TCNNQ recorded at different temperatures (80K, 130K, 180K, 230K, 280K). The plot highlights the narrowing of the EPR line width with increasing temperature as a result of motional narrowing.

SI-12 Grazing-incidence wide-angle x-ray scattering (GIWAXS) analysis

To determine the effect of doping on the ZnPc microstructure, we investigated the crystalline structure of both pure and 3 wt.% doped ZnPc film further analysing the Grazing Incidence Wide Angle X-ray Scattering (GIWAXS) measurements, previously published in ref[11] (Figure SI14). The GIWAXS analysis highlights the presence of crystalline grains both in the pure and doped films. The position of the Bragg peaks indicates two preferred crystallite orientations, with the out-of-plane peak corresponding to upright standing molecules and the in-plane peaks corresponding to lying down molecules. The higher intensity of the out-of-plane peak indicates that more crystalline grains are composed of molecules that approximately are aligned perpendicular to the substrate. The presence of dopant molecules is found to lead to the disappearance of higher order peaks and to decrease the crystallite size. In fact, through the Scherrer analysis we observed that the lower bound estimate of the crystallite size is 20.4 nm and 18.9 nm for the pure and doped ZnPc, respectively.

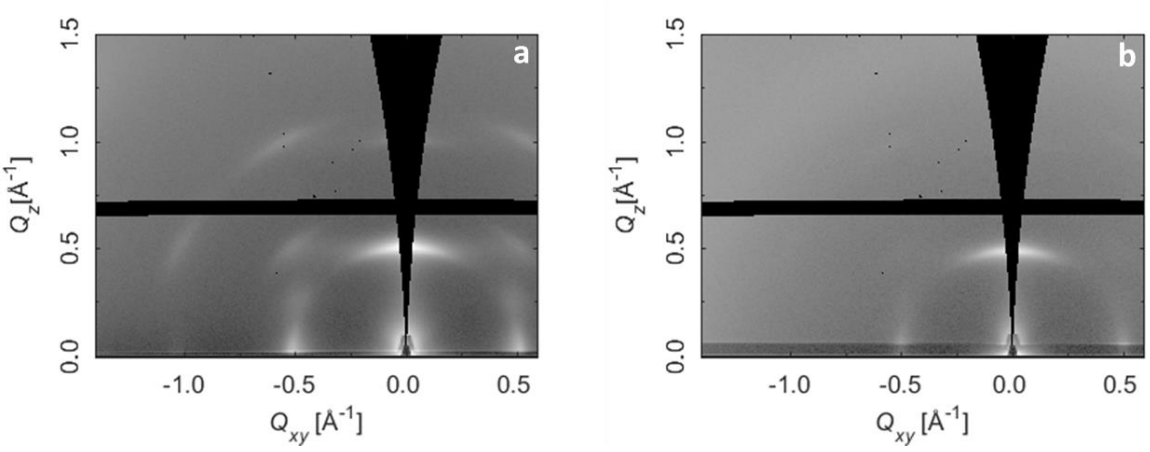

Figure SI17: GIWAXS 2D reciprocal space maps of (a) pure ZnPc and (b) ZnPc doped with F6-TCNNQ (3 wt%, MR=0.052) on SiO_2. The film thickness is 30 nm. All films display two preferred orientations either fully in-plane or fully out-of-plane, as seen by the (200) peak, with the out-of-plane orientation being the strongest, indicating a preference for edge-on orientation as compared to a lying-down orientation. A mosaic broadening is present in both cases, as is typical for organic thin films. The peak position values were derived from fitted line cuts through 2D GIWAXS images in the near out-of-plane direction through the (200) Bragg peak using a simple sector integration between 7° and 8° from the out-of-plane axial orientation. Lower bound estimates of the crystallite grain size were derived using the Scherrer equation:$\tau = \frac{K\lambda}{\beta\cos(\theta)}$, using a shape factor K=0.9 under the simple assumption of spherical crystallites.[15] The GIWAXS data have been already published in ref.[11]

Bibliography

1. S. Schaefer, PhD, Freie Universität Berlin, 2010.
2. A. Jha, H. G. Duan, V. Tiwari, M. Thorwart and R. J. D. Miller, *Chem Sci*, 2018, **9**, 4468-4476.
3. A. L. Sutton, B. F. Abrahams, D. M. D'Alessandro, T. A. Hudson, R. Robson and P. M. Usov, *CrystEngComm*, 2016, **18**, 8906-8914.
4. G. R. Eaton, S. S. Eaton, D. P. Barr and R. T. Weber, *Quantitative EPR*, Springer Vienna, 2010.
5. M. L. Tietze, J. Benduhn, P. Pahner, B. Nell, M. Schwarze, H. Kleemann, M. Krammer, K. Zojer, K. Vandewal and K. Leo, *Nat Commun*, 2018, **9**, 1182.
6. H. Kleemann, C. Schuenemann, A. A. Zakhidov, M. Riede, B. Lüssem and K. Leo, *Org. Electron.*, 2012, **13**, 58-65.
7. M. Kröger, S. Hamwi, J. Meyer, T. Riedl, W. Kowalsky and A. Kahn, *Org. Electron.*, 2009, **10**, 932-938.
8. S. D. Ha, J. Meyer and A. Kahn, *Phys. Rev. B*, 2010, **82**, 155434.
9. J.-H. Lee, H.-M. Kim, K.-B. Kim and J.-J. Kim, *Org. Electron.*, 2011, **12**, 950-954.
10. K. Kang, S. Watanabe, K. Broch, A. Sepe, A. Brown, I. Nasrallah, M. Nikolka, Z. Fei, M. Heeney, D. Matsumoto, K. Marumoto, H. Tanaka, S.-i. Kuroda and H. Sirringhaus, *Nature Materials*, 2016, **15**, 896-902.
11. R. Warren, A. Privitera, P. Kaienburg, A. E. Lauritzen, O. Thimm, J. Nelson and M. K. Riede, *Nat Commun*, 2019, **10**, 5538.
12. J. Li, I. Duchemin, O. M. Roscioni, P. Friederich, M. Anderson, E. Da Como, G. Kociok-Köhn, W. Wenzel, C. Zannoni, D. Beljonne, X. Blase and G. D'Avino, *Materials Horizons*, 2019, **6**, 107-114.
13. M. L. Tietze, P. Pahner, K. Schmidt, K. Leo and B. Lüssem, *Adv. Funct. Mater.*, 2015, **25**, 2701-2707.
14. B. Maennig, M. Pfeiffer, A. Nollau, X. Zhou, K. Leo and P. Simon, *Phys. Rev. B*, 2001, **64**.
15. A. L. Patterson, *Physical Review*, 1939, **56**, 978-982.